Dyes and Pigments 153 (2018) 106–116

Contents lists available at ScienceDirect

Dyes and Pigments

journal homepage: www.elsevier.com/locate/dyepig

Synergistic effect of supported ZnO/Bi_2O_3 heterojunctions for photocatalysis under visible light

J.C. Medina[a,b,*], N.S. Portillo-Vélez[a], M. Bizarro[b], A. Hernández-Gordillo[b,1], S.E. Rodil[b]

[a] Centro de Ciencias Aplicadas y Desarrollo Tecnológico, Universidad Nacional Autónoma de México, Circuito Exterior S/N, Ciudad Universitaria, A.P. 70-186, Delegación Coyoacán, C.P. 04510, Cd. Mx. México

[b] Instituto de Investigaciones en Materiales, Universidad Nacional Autónoma de México, A. P. 70-360, Coyoacán, C.P. 04510, Cd. Mx. México

ARTICLE INFO

Keywords:
ZnO/Bi_2O_3 heterojunction
Synergistic effect
Indigo carmine degradation
Visible light

ABSTRACT

In this article we report a novel and affordable approach to fabricate supported ZnO/Bi_2O_3 heterostructures for the visible-light photocatalytic degradation of organic compounds. This 2D-heterojunction was produced by depositing Bi_2O_3 dots by sputtering onto a ZnO thin film deposited on glass substrates by spray pyrolysis. The structural, morphological, electronic and optical properties were studied and characterized by X-ray diffraction (XRD), scanning electron microscopy (SEM), electrochemical impedance and UV–vis spectroscopy, respectively. Chemical composition spectra and images of the interface were obtained by X-ray photoelectron spectroscopy (XPS). Photocatalytic experiments were performed for the degradation of indigo carmine (IC) under UV and visible light irradiation, whilst the percentage of mineralization was measured by total organic content determination. It was found that the ZnO/Bi_2O_3 bi-layers with heterojunction showed enhanced photodiscoloration and mineralization under visible light compared to the ZnO and Bi_2O_3 films separately. This is due to a synergistic effect in which Bi_2O_3 extends the absorption range of the film to the visible region and the proper alignment of the electronic band edges induces charge separation with the subsequent reduction in the recombination rate. Moreover, through a careful analysis of the absorbance spectra of the IC dye solutions and the energetics for the different photocatalytic reactions, the mechanisms for the degradation routes followed under each irradiation source and material is proposed.

1. Introduction

Among different semiconductor materials, zinc oxide (ZnO) has been known as an outstanding photocatalyst for water treatment [1,2] having an important performance in the degradation and mineralization of several organic pollutants [3] [4–6]. However, some drawbacks have already been identified: ZnO is only active under UV radiation, it suffers from fast recombination of the electron-hole (e^--h^+) pairs and photocorrosion under UV irradiation and acidic conditions [1]. Up to now, three major strategies have been developed aiming to improve the photocatalytic efficiency, the stability and to extend the absorption of the semiconductor to the visible range: (i) additions of dopants (anionic, cationic or rare earth elements) [1], (ii) surface modification with noble metal nanoparticles [7,8] and (iii) the formation of heterojunctions with other semiconductors [1,9–11]. In this research work, we have chosen the coupling of two semiconductors since it looks as a promising strategy using available and non-expensive materials. By performing appropriate band engineering, it could be effective to extend the spectral response into the visible light and favor the charge separation and transport, avoiding recombination of the carriers. An adequate candidate is bismuth oxide (Bi_2O_3), which is non-toxic, chemically stable and abundant material in our country, but also because the optical band gap can be tuned between 1.7 and 3.9 eV according to the crystalline phase produced among its six possible polyphorms (α, β, γ, ε, ω and δ) [12–19]. The most studied phase is the room temperature stable α-Bi_2O_3 (optical gap 2.8 eV), which is usually obtained as micro-sized particles by chemical routes showing interesting photocatalytic performance under visible light [20,21]. On the other hand, the metastable tetragonal beta phase has been obtained as nanostructures (optical gap 2.4-2.8 eV) showing promising photocatalytic activity [22–25]. In the thin film form, it has been possible to obtain the β-phase [26] and the delta-phase [27,28], which is the high temperature Bi_2O_3 stable phase and well-known for its intrinsic ionic conductivity. In previous works, we demonstrated the potential properties of the δ-

* Corresponding author. Centro de Ciencias Aplicadas y Desarrollo Tecnológico, Universidad Nacional Autónoma de México, Circuito Exterior S/N, Ciudad Universitaria, A.P. 70-186, Delegación Coyoacán, C.P. 04510, Cd. Mx. México.
E-mail address: juan.medina@ccadet.unam.mx (J.C. Medina).
[1] CONACYT Research Fellow.

https://doi.org/10.1016/j.dyepig.2018.02.006
Received 25 November 2017; Received in revised form 3 February 2018; Accepted 4 February 2018
Available online 07 February 2018
0143-7208/

Bi_2O_3 thin films as visible-light photocatalytic material [16]. Nevertheless, further experiments showed that despite the large capability to induce the discoloration/degradation of textile dyes, the final degradation or mineralization of the organic molecules was not achieved [16,27,29]. A possible explanation is that the electronic band alignment allows the effective generation of superoxide radicals ($O_2^{\bullet-}$) which are able to break the azo bonds but due a high recombination, the subsequent reaction with water to produce hydroxyl radicals (·OH) is not completed.

Due to the visible-light absorption of Bi_2O_3 and the observed fast discoloration [14,21,22,25,30–33], some groups have already attempted to improve the photocatalytic properties of ZnO in the visible range by producing ZnO/Bi_2O_3 heterojunctions. Balachandran and Swaminathan [34] produced ZnO with 6.8–18.9 wt% of α-Bi_2O_3 nanostructures and showed that the discoloration rate under UV excitation was higher for the heterojunction (4 g/L of catalysts and 3×10^{-4} M of acid black) in comparison to the single oxides, no results for the visible light were presented. Wang et al. [35] produced ZnO/α-Bi_2O_3 heterojunctions by solid state reaction and showed that the 5% molar ratio ZnO/Bi_2O_3 nanomaterial, exhibited the best photodiscoloration activity using solar radiation, explained in terms of effective separation of charge carriers. Moreover, by using electron and hole scavengers, they concluded that the ·OH radicals were the main active species for the discoloration. Yang et al. [36] produced ZnO nanofibers decorated with β-Bi_2O_3 nanoparticles and showed improved photodiscoloration of RhB (1×10^{-5} M) for both UV and visible light, although for the visible light, a strong contribution from the dye photosensitization was observed. On the other hand, the creation of heterojunctions formed by ZnO and Bi_2O_3 anchored to a substrate, i. e. as thin films, has also been explored by B. Ling et al. [37], who reported the hierarchical growth of ZnO/β-Bi_2O_3 nanostructures by vapor-phase transport (VPT) on Si substrates but no photocatalytic evaluation was presented. C. Li et al. [38] synthesized ZnO/Bi_2O_3 heterojunctions by combining sol-gel deposited ZnO films on glass substrates with the deposition of an array of β-Bi_2O_3 by sputtering using a microsphere lithography strategy. High discoloration rates and total organic carbon reduction were only observed after the addition of Ag nanoparticles that functioned to avoid electron-hole recombination.

As can be seen from this short review of the backgrounds, the ZnO/Bi_2O_3 heterojunctions are based on α-Bi_2O_3 or β-Bi_2O_3 phases that have optical gaps of 2.8 and 2.4 eV, respectively. In the present work, we reported the creation of a ZnO/Bi_2O_3 heterojunction, where the low band gap cubic δ-Bi_2O_3 is used. This lower band gap could enhance the photocatalytic activity under visible light irradiation. Two deposition methods were used; the ZnO was deposited by spray pyrolysis and Bi_2O_3 by sputtering using a mask. The optical gap of the δ-Bi_2O_3 is 1.7 eV and its fast discoloration capacity under acidic conditions has already been proved [16,27]. The aim is to synergistically join the strengths of both semiconductors to achieve the mineralization of organic pollutants using visible light with the advantage of the easier handling and reusability of the supported photocatalytic material.

2. Experimental details

2.1. Thin films deposition

Firstly, pure ZnO thin films were obtained by pneumatic spray pyrolysis technique on corning glass substrates (2.5 × 1.25 cm). The spray system uses a 1/4JAU-SS air atomizing nozzle from Spraying Systems Co. placed at 30 cm from the substrate. The substrates were cleaned consecutively with trichloethylene, acetone and methanol for 5 min then were dried with compressed nitrogen. The precursor salt was Zinc Acetate 0.1 M ($Zn(CH_3COO)_2{\cdot}2H_2O$, 98% purity from Sigma-Aldrich) and deionized water was used as solvent. The substrates were heated at 450 °C previous to the deposition by placing the substrates on a tin bath. Then, gas and solution flow were initiated at a rate of 1024 ml/min and 5.5 ml/min, respectively during 15 min [39].

Afterwards, in a different deposition chamber, Bi_2O_3 dots (2 mm ∅) were deposited on the ZnO films by magnetron sputtering using a 10-holes aluminum-mask placed on top of the ZnO coating. The base pressure was 4×10^{-4} Pa and the deposition pressure was set at 2.67 Pa through the addition of an Ar:O_2 gas mixture at 80:20 flow rate ratio. The substrates were heated at 150 °C for 30 min before applying 100 W of radio frequency power to a 4″ circular α-Bi_2O_3 target during 10 min. These conditions led to the growth of 400 nm crystalline bismuth oxide delta cubic phase (δ-Bi_2O_3) dots [16,27].

2.2. Thin films characterization

The structure of the individual films was studied by X-ray diffraction (XRD) using a Rigaku Ultima IV system (CuKα 1.5406 Å, 40 kV, 44 mA and angle step of 0.02°) in the Bragg-Brentano configuration. The diffraction patterns were analyzed by the PDXL2 software to identify the phases and determine the grain size (Halder-Wagner method). Moreover, surface morphology of the individual films was observed by scanning electron microscopy (SEM) with a microscope JEOL model 7600F, whilst their optical properties were determined by optical transmittance experiments. In addition, the film thickness was measured using a Veeco Dektak 150 profilometer. The chemical composition of the heterojunction ZnO/Bi_2O_3 films was evaluated by X-ray photoelectron spectroscopy (XPS) using a Physical Electronics equipped with a scanning XPS microprobe PHI 5000 VersaProbe II detector. The measurements were done under ultrahigh vacuum 4×10^{-8} Pa, and the X-ray source was of Al Kα ($h\nu = 1486.6$ eV). The survey spectra were recorded with 100 eV energy steps, and the high-resolution spectra at 20 eV. The spectra were analyzed before and after Ar^+ cleaning. The spurious C1s signal at 285 eV was used to correct the binding energies. The Ar cleaning was done for 3 min using low energy (1 keV) and low current (55.6 nA/m^2) to avoid modification of the oxidation state for both Zn and Bi. The data was analyzed using the Multipack© version 9.6.0.15 software. To obtain information about the band edge positions, the coatings (ZnO and δ-Bi_2O_3) were deposited on a transparent conductive oxide coated glass and Mott-Schottky measurements at different frequencies were performed using a three electrode cell (Platinum, Ag/AgCl and the sample).

2.3. Photocatalytic activity experiments

The photocatalytic activity of the films was evaluated by measuring the evolution of the absorbance spectrum of a 5 mg/L (1×10^{-5} M) aqueous solution of indigo carmine dye (IC, $C_{16}H_8N_2Na_2O_8S_2$) as a function of the irradiation time. Each film (3.125 cm^2) was immersed in 10 ml of the dye solution and exposed to different light sources: (i) UV light (9 W fluorescent lamp with main emission peak centered at $\lambda = 368$ nm) and (ii) white light (9 W fluorescent lamp with no UV contribution, $\lambda > 400$ nm). The concentration used was chosen considering that the amount of catalyst deposited on a 3.125 cm^2 glass substrate is relatively small (less than 1 mg), so it is not possible at this scale to work with larger concentrations. Nevertheless, the estimated grams of catalyst per mole of pollutant are comparable or even larger to those commonly reported for powder samples [14,40–44].

During the experiment, the solution was kept under magnetic stirring at 1600 revolutions per minute to enhance the oxygenation of the solution and to assure that the reaction remains on the kinetic regime. The solution was used at room temperature and without any pH adjustment (pH = 7). Initially, the solution was kept under dark conditions and the absorbance of the solution was monitored from time to time until no further changes were observed, indicating that the adsorption-desorption equilibrium was reached. It was shown that for all the experiments, an initial time of 30 min in the dark was enough to reach the equilibrium. Then, illumination was started followed by measurements of the absorption spectra of the solution every 30 min

taking aliquots of 3 mL. The absorbance spectra were measured using a 1800 UV-vis Shimadzu spectrophotometer and the aliquots were returned to the vial after each measurement to continue the experiment up to 3 h. The discoloration efficiency of the solution was obtained as follows:

$\%\ \text{Discoloration} = \left(1 - \frac{C}{C_o}\right) \times 100$ where C_o and C are the absorbance maxima of the IC solution before and after the irradiation time, respectively.

The reaction rate constant, under UV light conditions, was calculated by using the Langmuir-Hinshelwood model, considering first order reaction, $Ln\left(\frac{C_o}{C}\right) = K_{app}t$. Plotting Ln ($C_o/C$) versus reaction time ($t$) leads to a straight line, and the slope corresponds to the apparent kinetic rate constant (K_{app} in min^{-1}).

Meanwhile, for the white light illumination, the reaction was better described by a zero order model, $C = C_o + k_o t$, where the reaction rate constant is independent of the initial concentration of the dye solution. Then, plotting C versus reaction time (t) yields to a straight line and the slope is the zero order kinetic rate constant (k_o in M min^{-1}).

The mineralization occurs by oxidative process with reactive oxygen species or by direct attack of the photogenerated holes to the organic molecules, degrading the dye molecule into intermediate compounds and subsequently into CO_2 and H_2O following equation: IC → Intermediates → CO_2 + H_2O

The percentage of total organic carbon reduction was estimated from the variation between the initial and final total organic carbon (TOC) content in the dye solution: $\text{Mineralization} = \left(\frac{\text{TOC}_{\text{initial}} - \text{TOC}_{\text{final}}}{\text{TOC}_{\text{initial}}}\right) * 100\%$.

The TOC measurements were recorded in a TOC-L Shimadzu equipment with a high sensibility column.

The production of hydroxyl radicals by the films as a consequence of the electron-hole production during irradiation was determined using a coumarin aqueous solution (0.05 M). For this, the films were immersed in the coumarin solution and irradiated for 60 min. Immediately, an aliquot was extracted to measure the fluorescence spectrum using a spectrofluorometer Fluorolog3 Horiba with Xe lamp (λ = 350 nm). The fluorescence signal is produced by the complex known as 7-hydroxycoumarin formed by reaction of hydroxyl radicals with coumarin. The 7-hydroxycoumarin complex exhibits a fluorescence emission signal at 454 nm [29], and the luminescence intensity is proportional to the amount of hydroxyl radicals that were produced by the semiconductor.

3. Results

Under the selected deposition conditions, the thickness measured by profilometry of the sprayed ZnO film was of 570 nm and 400 nm for the Bi_2O_3. Since the Bi_2O_3 dots were deposited on top of the ZnO surface, the final film exhibited a thickness profile where the zones of the sputtered dots had a higher thickness that the rest of the ZnO film.

3.1. Structure

Fig. 1 shows the Bragg-Brentano XRD patterns of the individual semiconductors and the bi-layer (ZnO/Bi_2O_3) film. The XRD pattern of the pure ZnO film (Fig. 1a) exhibited the presence of the hexagonal wurtzite phase with diffraction peaks at 31.77, 34.42, 36.25, 47.54 and 56.60, corresponding to the planes (100), (002), (101), (102) and (110) respectively and according to the PDF 00-036-1451. The relative intensities of the diffraction peaks of the ZnO films are different to those expected for the powder diffraction pattern, indicating the development of preferred orientation during film growth. The average crystalline domain size was 38 nm.

Fig. 1b shows the diffractogram of a continuous Bi_2O_3 film deposited on glass under the same deposition conditions as the dots. The pattern consists of five characteristic diffraction peaks of the δ-cubic

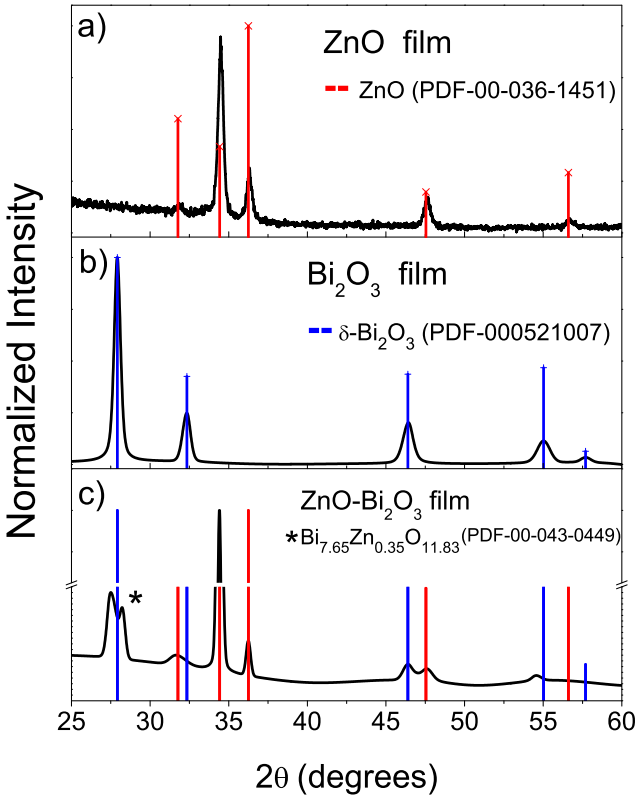

Fig. 1. X-ray diffraction patterns of a) ZnO thin film, b) Bi_2O_3 thin film c) ZnO/Bi_2O_3 thin film.

phase (PDF-00-052-1007); (111), (200), (220), (311) and (222) that we have already shown [16,27,45,46] can be obtained on different substrates as far as the deposition conditions (RF power and substrates temperature) are properly controlled. No preferred orientation was observed, allowing a confident identification of the δ-Bi_2O_3 phase. The crystalline domain size of the δ-Bi_2O_3 was 17 nm.

Finally, the diffraction pattern obtained from a ZnO-Bi_2O_3 bi-layer film (Fig. 1c) shows evidence of both single oxides. The predominant signal on the pattern is from the ZnO in agreement with the lower volume corresponding to the Bi_2O_3 dots; the analyzed area contains a larger fraction of ZnO (~90%) in comparison to the area occupied by the Bi_2O_3 dots (~10%). The Bi_2O_3 diffraction peak around 28°, which is actually the most intense of the δ-Bi_2O_3 phase, shows a minor reflection that might be related to a Bi-Zn-O compound, as could be identified by the database as $Bi_{7.65}Zn_{0.35}O_{11.83}$ (PDF-00-043-0449). However, only one peak was observed making difficult a proper identification.

The surface morphology of the individual films and the heterojunction can be observed in Fig. 2a–c. Fig. 2a shows that the ZnO film is composed of randomly oriented nanoflakes. Other surface morphologies, more ordered and oriented can also be obtained; however, in a previous work, we have shown [39] that the photocatalytic properties were enhanced for the irregular topography used in this work. Fig. 2b shows the nanosize granular shape of the δ-Bi_2O_3 single dots deposited by magnetron sputtering, similar to our previous reports [16,27,45,46]. Fig. 2c shows a low resolution secondary-backscattering electron image of the ZnO/Bi_2O_3 bi-layer film-surface in order to observe the compositional contrast at the border of an individual Bi_2O_3 dot. The region presenting a brighter contrast corresponds to the Bi_2O_3 and is due to the larger atomic mass of Bi in comparison to Zn.

3.2. Elemental composition

The composition of the ZnO/Bi_2O_3 bi-layer film was analyzed by XPS using a chemical composition image (X-ray beam induced

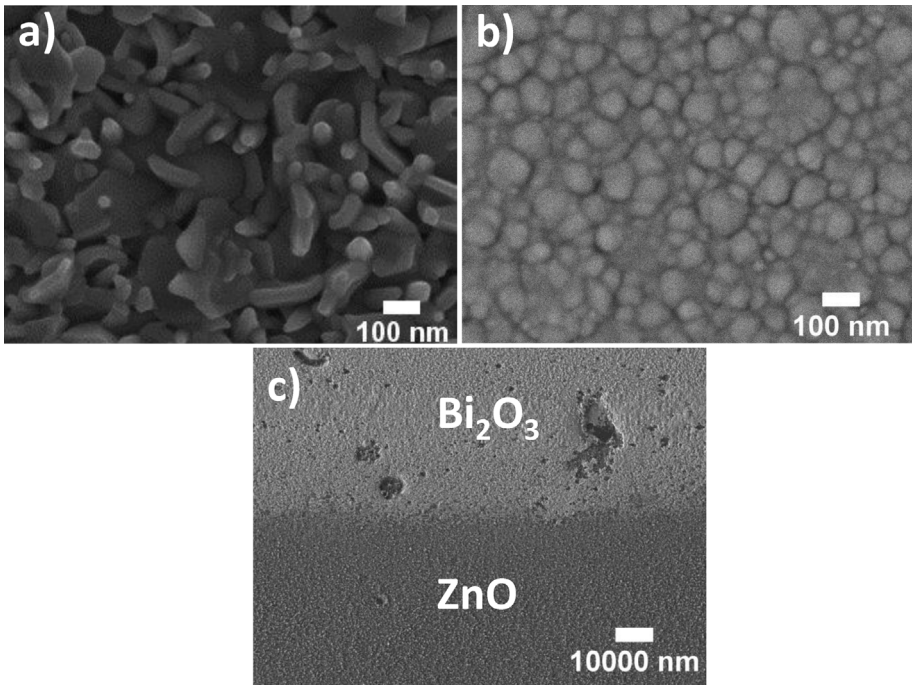

Fig. 2. Secondary electron image of the a) ZnO thin films and b) Bi_2O_3 thin films. c) Low resolution mixed secondary and backscattered electron image of the border of one of the Bi_2O_3 dots on the ZnO film.

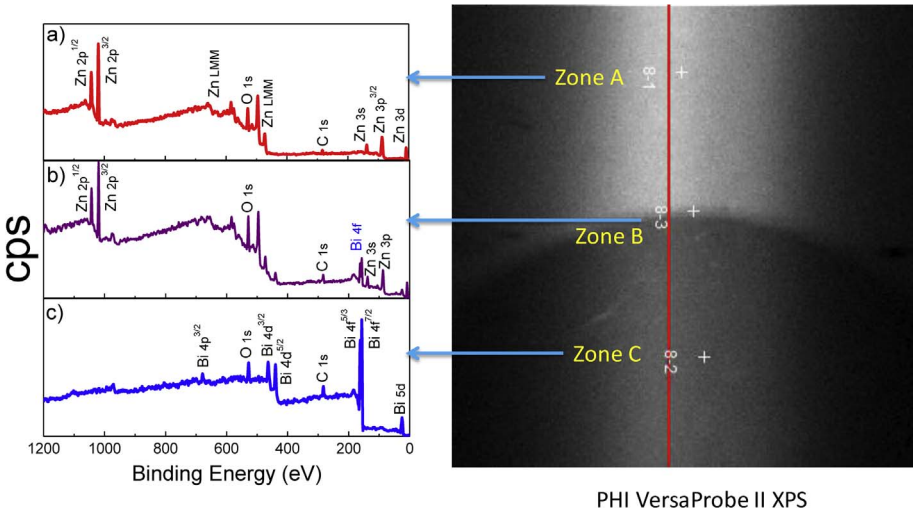

Fig. 3. Survey XPS spectra for the different zones indicated in the SXI image: a) Zone A, ZnO film, b) Zone B, ZnO/Bi_2O_3 heterojunction and c) Zone C, Bi_2O_3 dot.

secondary electron image, SXI) and selected area (10 μm) spectra, as shown in Fig. 3. The SXI image (1400 × 1400 μm) shows a clear contrast between the border of a Bi_2O_3 dot and the underlying ZnO film. Three spectra were collected in the zones indicated (A, B and C) in the image to demonstrate the differences in the chemical composition observed in the SXI-image and the SEM (Fig. 2c). The results showed that apart from the small signal of spurious carbon, in spectra A only photoemission peaks from Zn and O were detected corresponding to the ZnO film, while at the interface (spectra B) signals from Zn, O, and Bi were detected and, finally inside the Bi_2O_3 dot (spectra C) only photoemission from Bi and O are observed. The spectra shown in Zone B correspond to the ZnO/Bi_2O_3 heterojunction in which both oxides are in close contact allowing charge transfer between them. It is not possible to define precisely the corresponding volume of the ZnO/Bi_2O_3 heterojunction, but it should be only a thin donut region in the perimeter around the 10-Bi_2O_3 dots.

3.3. Optical properties

Fig. 4 shows the optical absorbance spectra of the individual ZnO and Bi_2O_3 films in comparison to the ZnO/Bi_2O_3 bi-layer film. The Bi_2O_3 film shows larger optical absorption for energies above 2.0 eV in comparison to the ZnO, reflecting the different optical band gaps. For the bi-layer film, the absorbance is between that of the individual materials, not completely dominated by the more absorbing Bi_2O_3. The absorbance spectra show long absorption tails below the absorption edge for both oxides, indicating the contribution of band-tail electronic states [47]. This is characteristic of the deposition methods [27,48,49] and the fact that the crystalline domain for both films is nanometric and therefore, there is a large fraction of grain boundary contribution to the optical-electronic properties. These band tail states are responsible for the slight light absorption and electron-hole pair creation of the ZnO film under visible light. Fig. 4 also includes the visible lamp emission used for the photocatalytic experiments.

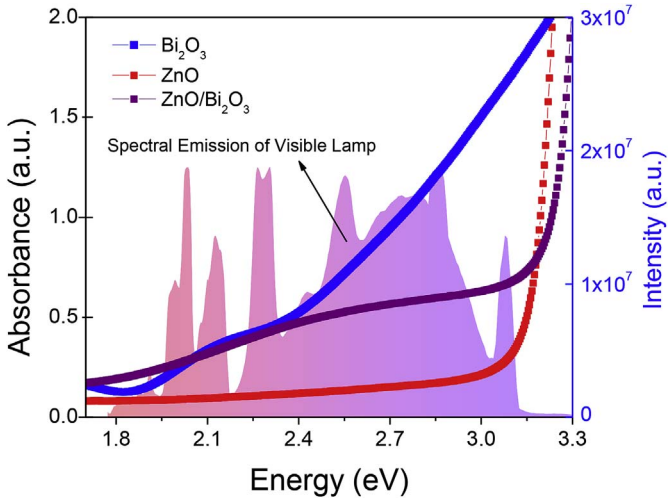

Fig. 4. Absorbance spectra measured for the samples deposited on glass and spectral emission of visible light lamp used in the photocatalytic experiments.

As a first approximation, the absorption coefficient (α) was determined from the transmittance spectra of the ZnO and Bi_2O_3 films in order to estimate their optical band gap, E_g. The E_g was estimated using the standard relation: $\alpha h\nu = A(h\nu - E_g)^n$ where A is a constant, h is Planck's constant, ν is the photon frequency, E_g is the optical band gap, and n = 1/2 for direct band gap semiconductors whilst n = 2 for indirect band gap semiconductor. In Fig. 5 it can observe that plotting $(\alpha h\nu)^{1/n}$ versus the photon energy, hν and extrapolating the linear part of the curve to zero gives the value of the optical band gap. The results indicate that the direct optical gap for ZnO is E_g = 3.2 eV in agreement with reported values [48,50]. Whilst for the δ-Bi_2O_3 samples, an indirect gap was used leading to E_g equal to 1.75 eV, in good agreement with previously reported values for this Bi_2O_3 phase [16,27,28,51].

3.4. Photocatalytic activity of the samples

The relative profile concentration (C/C_o) of the Indigo Carmine (IC) dye during the photolysis and photocatalytic reaction at pH = 7 are shown in Fig. 6a–b for the individual ZnO, Bi_2O_3 dots and the bi-layer film. As mentioned above, the adsorption-desorption equilibrium was already reached after 30 min, therefore, the C/C_o plots include the initial dye concentration (C/C_o = 1), the data after 30 min kept in the dark while stirring (time = 0) and the values after illumination.

For UV (Fig. 6a) and white (Fig. 6b) illumination, it can be observed that during the dark conditions, the dye concentration did not decrease indicating that the dye adsorption on the films surface is negligible. Moreover, the photolysis included for both illuminations show only a minor C/C_o decrement for the white light, validating the stability of the IC dye during irradiation. The confirmation of non-dye adsorption on the surface of the films and negligible photolysis, allow us to categorize the decrease in time of the C/C_o ratio as a discoloration process consequence of the photocatalytic activity driven by the semiconductor material.

Under UV illumination using the Bi_2O_3 dots, it is observed that the C/C_o of the dye is only slightly decreased, i. e. the discoloration induced by the Bi_2O_3 dots is very small respect to the photolysis, this is explained for the small amount of material and also because the Bi_2O_3 films presented the maximum discoloration rates at acidic and not at neutral pH as it has been shown previously [27]. Meanwhile, the pure ZnO film and the ZnO/Bi_2O_3 bi-layer attained a full discoloration of the IC dye in a short time (60 min). The apparent kinetic rate constant (K_{app}) estimated using the pseudo first order model was 0.05 min^{-1} for both ZnO and ZnO/Bi_2O_3 films. According to these results, it can be concluded that there is no clear advantage of using the bi-layer films containing the heterojunctions under the UV illumination and that both films followed the same mechanism to achieve the photodiscoloration of the dye.

A different scenario was observed for the white-visible light illumination, firstly, the photocatalytic response needs to be monitored for a longer time; up 180 min, as is presented in Fig. 6b and secondly, a different mechanism was envisioned. The Bi_2O_3 dots induced only a slight decrease of the IC dye concentration, while the ZnO/Bi_2O_3 showed the largest photocatalytic activity, even superior to the pure ZnO film. The linear tendency in the C/C_0 plot clearly indicated a zero order kinetic-regime, where the discoloration reaction rate is independent of the concentration of the dye. The zero order kinetic rate constants obtained for ZnO and ZnO/Bi_2O_3 are 0.17 and 0.23 $Mmin^{-1}$, respectively, showing that the bi-layer film containing the heterojunctions was 35% more efficient than ZnO, effect that is representative of a synergistic effect.

The recyclability of the bi-layers containing the ZnO/Bi_2O_3 heterojunctions was evaluated by repeating the photocatalytic experiment reusing the same film for three cycles of 330 min each.

Fig. 7 shows that under white light and after three cycles, the photocatalytic efficiency of the ZnO/Bi_2O_3 bi-layer film remained practically constant. After the cycles the film did not suffer damage or detachment from the substrate.

The TOC of the dye aqueous solutions were measured after the discoloration reaction time and it was compared with the initial TOC contained in the original solution dye, giving the percentage of mineralization. Fig. 8 shows the results of mineralization (%) obtained under UV and white light irradiation for ZnO and the heterojunction.

The mineralization percentages after 180 min using the UV light were 60 and 50% for ZnO film and ZnO/Bi_2O_3 film, respectively. Meanwhile, for the visible light, the reaction time was prolonged up to 720 min due to the lower reaction rate, but interestingly, the percentage of mineralization was significantly higher for the ZnO/Bi_2O_3 bi-layer containing the heterojunction (43%) in comparison to the pure ZnO

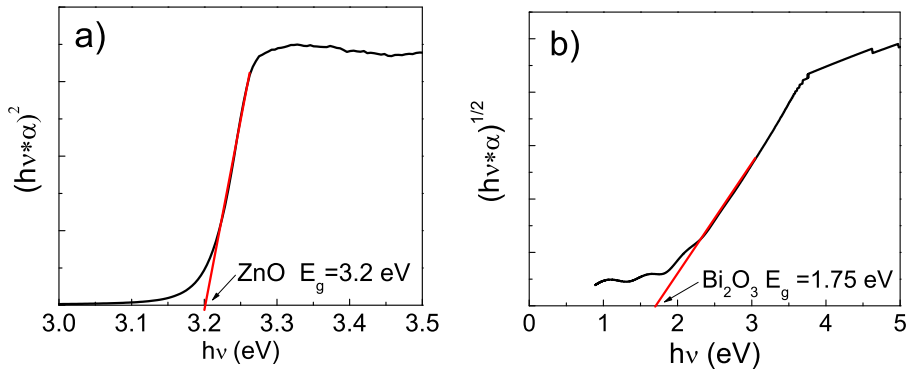

Fig. 5. Determination of the band gap obtained by optical transmission measurements for a) ZnO and b) Bi_2O_3 films.

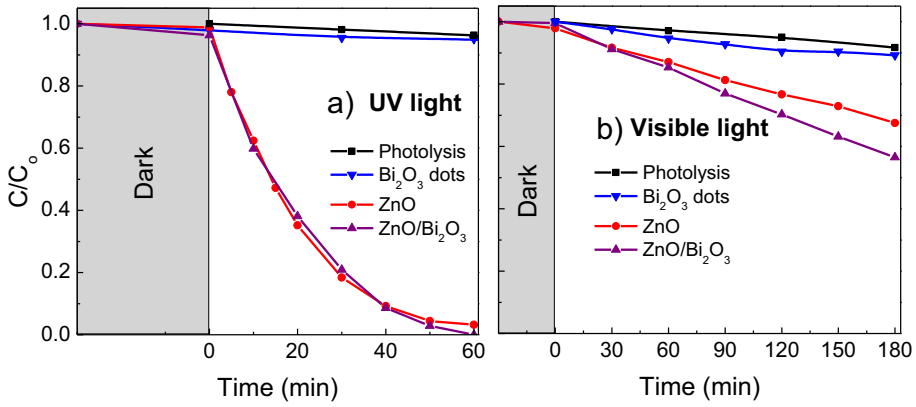

Fig. 6. Evaluation of the photocatalytic activity for Bi_2O_3 dots, ZnO film and ZnO/Bi_2O_3 films under a) UV light and b) visible light.

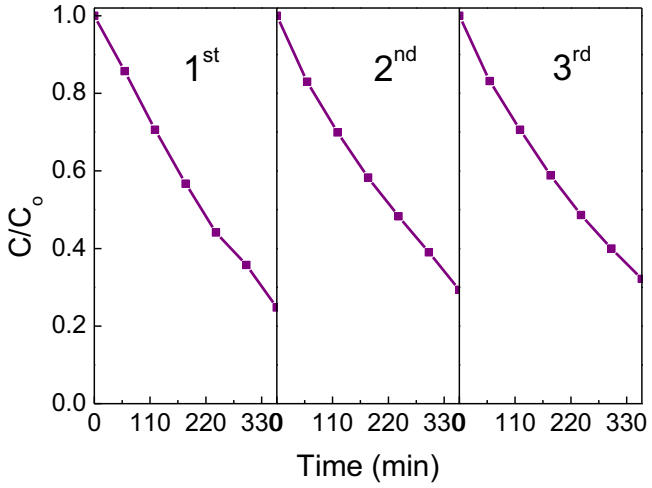

Fig. 7. Degradation test of IC solution under visible light after three cycles.

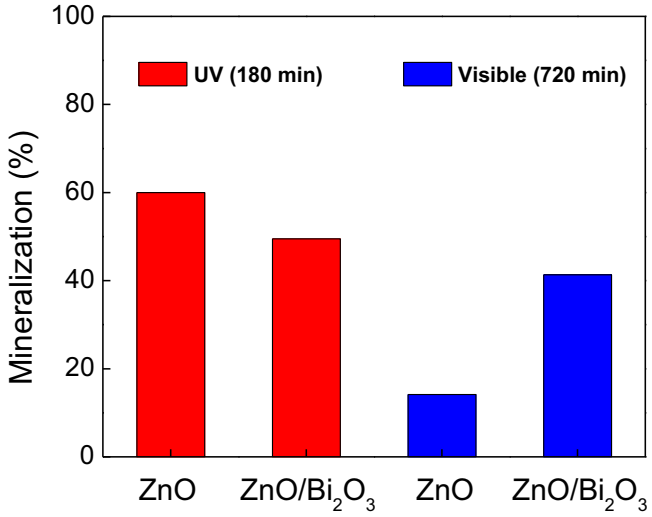

Fig. 8. Mineralization percentage of IC solution by ZnO and ZnO/Bi_2O_3 films using different lights.

(17%). Therefore, it can be observed that a significantly important fraction of mineralization could be achieved using the heterojunctions under visible light. This high mineralization percentages are obtained after the discoloration process of the dye toward CO_2 mineral, which indicates that IC dye was degraded through the chemical reactivity of hydroxyl radicals, following the degradation pathway of organic molecules extensively reported [52,53]. Therefore from now on, we can certainly speak of the photodegradation of the IC dye due to the photocatalytic activity of the semiconductor films.

In order to get a measure of the relative amount of hydroxyl radicals for each sample, we evaluated the production of ·OH radicals under different illumination regimes using the photoluminescence (PL) signal from the 7-hydroxycoumarin complex, as shown in Fig. 9. The PL spectra in Fig. 9 show two signals: one at 390 nm that corresponds to the coumarin in solution and therefore is observed for all samples and the other at 454 nm related with the emission of 7-hydroxycoumarin complex, which is mainly observed for the ZnO and the heterojunction films. The low intensity of the 454 nm signal for the Bi_2O_3 dots film suggests that there is a scarce hydroxyl radical production. On the other hand, using pure ZnO and ZnO/Bi_2O_3 films, the 454 nm is significantly increased after illumination confirming the formation of the 7-hydroxycoumarin complex due to the effective production of hydroxyl radicals. The amount of ·OH radicals is lower under visible-light than UV-light, but the difference between ZnO and the bi-layer films follows the same proportion. Moreover, the data shows that the PL intensity, and therefore the fraction of hydroxyl radicals formed at 60 min, is always larger on the ZnO than in the ZnO/Bi_2O_3 bi-layer film. This result might seem inconsistent with the mineralization values (Fig. 8), which indicated a larger mineralization of the bi-layer films, since the highly reactive ·OH are considered the main active species responsible for the mineralization. However, it is because, we did only measure the OH production at a single illumination time and there is no specific correlation between the ·OH concentration and photodegradation. Diverse authors [29,54,55] have demonstrated, instead, a linear correlation between the photodegradation and the ·OH *formation rate*, which we do not measure in this work.

Our interest was to demonstrate that for both films, ZnO and the bi-layers, it was possible to form hydroxyl radicals under visible light and therefore explain the observed mineralization in Fig. 8. In the following sections, an explanation about the mechanism of formation of these hydroxyl radicals is discussed.

3.5. Mott Schottky

For in depth understanding the mechanism leading to photodegradation of the IC dye, the band edge position of the isolated coatings was obtained using the electrochemical impedance measurements in the dark. Using the Mott-Schottky (MS) plots, the flat band potential for the two oxides were obtained as shown in Fig. 10. It can be seen that both films are n-type semiconductors since the slope is positive, so the majority carriers are electrons. Fig. 10a shows the MS-plot for the ZnO film obtained at three different frequencies to corroborate that the flat band potential is -0.13 V_{NHE} pH ~ 7, which is different to the theoretical values reported in other works [9,56]. However, the

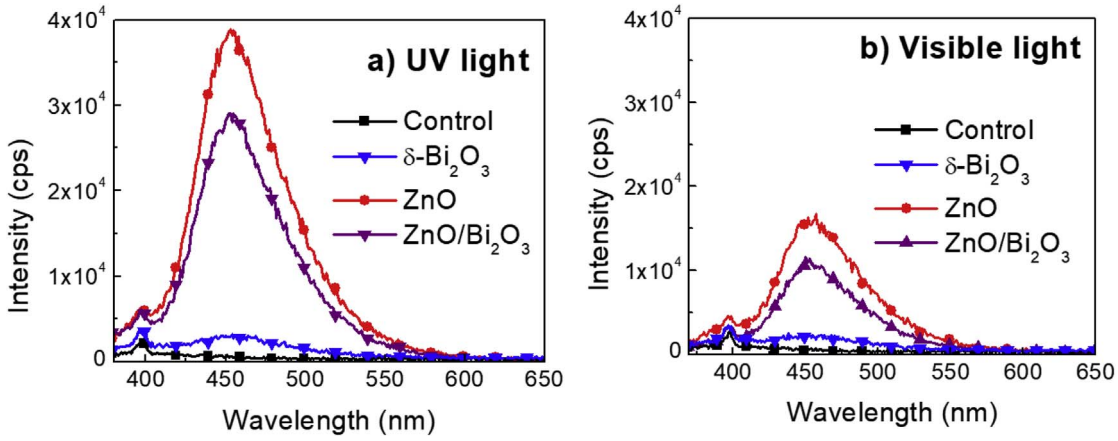

Fig. 9. Determination of ·OH radicals by ZnO, ZnO/Bi_2O_3 and Bi_2O_3 films using: a) UV light and b) visible light. Both measurements were done at pH 7 and during 60 min.

value is more similar to the experimental value reported by Karmakar et al. [57] (−0.23 V_{NHE}, pH ~ 6.5) who also explained that the flat band potential is very sensitive to the synthesis method and morphology of the samples. It is important to mention that the linear region to adjust the flat band potential for these ZnO films was not so well defined, so we choose the value with the best regression factor, selected from many other similar-size potential windows. The MS-plot of the bismuth oxide, δ-Bi_2O_3, is shown in Fig. 10b that shows that the flat band potential is −0.54 V_{NHE} at pH ~7, better defined than for the ZnO. No comparison with the literature is done, since previous works reported band edge position for other Bi_2O_3 crystalline phases.

4. Discussion

A novel method to synthesize a heterojunction between two different semiconductors like ZnO and Bi_2O_3, combining spray pyrolysis and magnetron sputtering techniques was presented in this study. We took advantage of the facility to obtain convenient morphologies of certain semiconductor oxides for photocatalytic applications by the spray pyrolysis technique and our previous knowledge of the Bi_2O_3 as a photocatalytic material to synthesize bi-layer films containing ZnO/Bi_2O_3 heterojunctions. The detailed analysis of the photodegradation kinetics and the mineralization (from TOC analysis) of the bi-layer films in comparison to the single oxides allow us to declare a synergetic positive collaboration of the ZnO/Bi_2O_3 heterojunctions, which leads to a ~100% photodegradation and 43% mineralization of the IC dye solution using a visible low power illumination lamp (33 W/m^2). This result is remarkable considering than previous works related to the use of ZnO-Bi_2O_3 heterojunctions have only demonstrated the photodiscoloration of dyes, and not the mineralization, using higher power lamps [14,22,30,31,33,38,40]. According to Hermann [58] for radiant flux below 250 W/m^2, the reaction rate is proportional to the radiant flux, so faster degradation and mineralization could be achieved by increasing the lamp power.

4.1. Band diagram and possible mechanism of IC dye degradation by ZnO/Bi_2O_3 films

In order to understand the results obtained under the visible light, the electronic band structure of both oxides was analyzed. For an n-type semiconductor, the flat band positions obtained by the MS plots, are equivalent to the band edge position (minimum energy) of the conduction band (CB) and the valence band (VB) top is situated at $E_{VB} = E_{CB} + Eg$.

Therefore the band diagram of the oxides at pH ~ 7 is as shown in Fig. 11a, which also include the redox potentials of the oxygen reduction reactions that might lead to the formation of reactive oxygen species (ROS) like superoxide radical ($O_2^{\cdot -}$), hydrogen peroxide (H_2O_2) and hydroxyl radicals (·OH) [59,60]:

(1) $H_2O + h^+ \rightarrow \cdot OH + H^+$ (+2.31 V)
(1a) $2H_2O + 4h^+ \rightarrow O_2 + 4\,H^+$ (+0.81 V)
(2) $O_{2\ (dissolved)} + e^- \rightarrow O_2^{\cdot -}{}_{(aqueous)}$, (−0.13 V)
(2a) $O_2^{\cdot -} + e^- + 2H^+ \rightarrow H_2O_2$ (+0.89 V)
(2b) $H_2O_2 + e^- + H^+ \rightarrow \cdot OH + H_2O$ (+0.38 V)

For the bi-layer films, the donut region around the Bi_2O_3 dots where the two oxides are in close contact, the electric field built at the interface between the two oxides controls the charge transfer between them. The position of the bottom of the CB of the Bi_2O_3 lower (more negative) than the ZnO is adequate for the occurrence of electron transfer, while the more positive top of the VB in ZnO will allow the

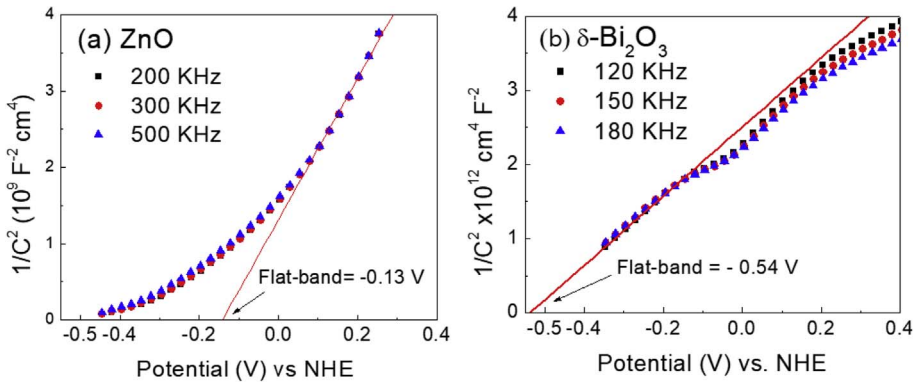

Fig. 10. Mott−Schottky plots measured in 0.5 M Na_2SO_4 (pH ~7) at different frequencies for: a) ZnO, b) δ-Bi_2O_3 films.

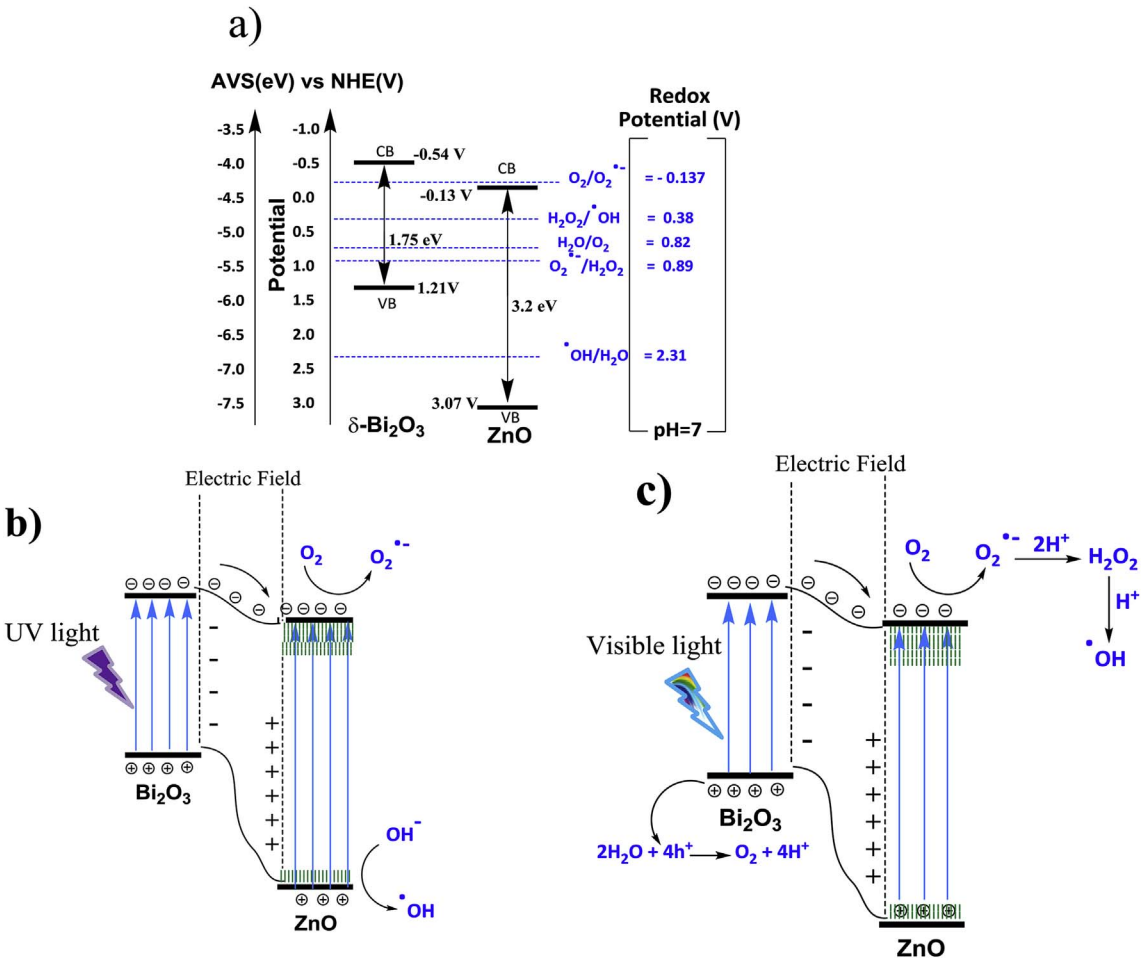

Fig. 11. a) Proposed band structures of the ZnO and Bi_2O_3 separately. The band diagrams and reactions after contact using b) UV light, c) visible light.

hole transfer towards the Bi_2O_3, these charge transfer processes that can occur only in the perimeter area around the Bi_2O_3 dots will reduce the recombination of the photocarriers generated within the individual semiconductors.

(i) When illuminated with the UV light (Fig. 11b), e^--h^+ pairs can be produced in both semiconductors and the photogenerated electron-hole pairs will be separated in the ZnO/Bi_2O_3 interface, increasing the lifetime of charge carriers and giving them enough time to react with the oxygen species adsorbed onto the photocatalyst surface to form the ROS. The holes in the ZnO-VB have enough potential energy to follow reaction (1) so there is a good production of hydroxyl radicals (·OH) for both the ZnO and the ZnO/Bi_2O_3 bi-layer films. Meanwhile, the electrons left in the ZnO-CB or the Bi_2O_3-CB could react with the dissolved oxygen (2) to produce superoxide radicals ($O_2^{\bullet-}$), which could either participate in the degradation process or continue with the reaction (2a) and (2b) to form more hydroxyl radicals (2b). These two sources of ·OH production lead to a very fast degradation reaction rate and high mineralization. However, there is no advantage for the use of the bi-layer films in comparison to pure ZnO.

(ii) Under visible illumination (Fig. 11c), the photocatalytic activity was not so fast since it occurred through a different mechanism than under UV-light and in this case, a clear advantage of using the ZnO/Bi_2O_3 heterojunctions was observed. Firstly, let us explain the photocatalytic results obtained for the pure ZnO films under visible-light illumination. It was shown that the ZnO films deposited by spray were able to induce photodegradation and a small fraction of mineralization under sub-gap illumination. There was also a clear signal of formation of ·OH radicals (Fig. 9), although the intensity of the PL signal was lower under visible than under UV-light. A possible explanation for the activity under sub-gap illumination comes from the contribution of the defects or band tail states [48]. Based on the lower photodegradation rate and zero-order kinetic regime observed for the ZnO under visible light, we propose that the photodegradation achieved was due to photocarriers produced due to transitions between localized ZnO-VB tail states to extended ZnO-CB states, as schematically shown in Fig. 11c. Under such transitions, the holes will remain localized (not available for reaction (1)), but the electrons could promote the formation of superoxide radicals following reactions (2). The photocatalytic effect of the localized-to-extended states will be comparable to that between extended-to-extended states since the transition probability have been shown to be similar in both cases [61]. Thus, under visible-light excitation, the photocatalytic activity (and the ·OH generation) of these ZnO films is explained through reactions (2) induced by the photoelectrons. The superoxide radicals produced are very effective oxidizing species which can break the azo bonds of many dyes [62]. Chen et al. [62] also demonstrated, by using different scavengers, that superoxides are the main reactive oxygen species for the degradation of azo dyes using Ag doped ZnO [7].

On the other hand, the pure Bi_2O_3 dots did not show any photocatalytic activity despite that it is easily activated by visible light, producing great amount of electrons and holes. However, the potential energy of the holes is not enough to induce reaction (1) and most probably the holes suffer recombination with the electrons instead of production of ·OH radicals through reaction (2) explaining that there is

neither ·OH signal nor mineralization.

When the two oxides are coupled in the bi-layer films containing the small volume of ZnO/Bi_2O_3 heterojunctions, a significant photodegradation and mineralization was observed under visible light illumination. Such results can be explained in terms of an improved charge separation leading to a vast amount of available electrons on the CB of both oxides for the production of ROS thorough reactions (2). Meanwhile, the holes in both oxides can produce H^+ through reaction (1a), and H^+ are consumed to complete reactions (2a-b). Therefore, the ~100% photodegradation achieved by the heterojunction under white illumination can be explained mainly because the superoxide radicals ($O_2^{\bullet-}$) are formed from electrons in the CB of ZnO and Bi_2O_3 following reactions (2). Due to the lower recombination, the reaction (2) continues to form ·OH radicals (2a-b), which eventually lead to the 43% mineralization.

The differences proposed in the formation of photocarriers and ROS between UV and visible light for the photocatalytic degradation of the IC dye has an impact on both the kinetics and the degradation of the dye. For the visible light, the reaction was slower and of zero order. Meanwhile the degradation path of the IC molecule was also different as could be observed by analyzing the full absorption spectra and discussed in the following section.

4.2. IC dye degradation by ZnO/Bi_2O_3 films

In the results section, it was shown that the degradation rate was much slower using visible light, but also followed a different kinetic regime. A careful analysis of the absorbance spectra to observe the different degradation mechanism can be seen in Fig. 12 for both lights.

Fig. 12a shows the absorbance spectrum of the IC dye solution as a function of UV irradiation time. This spectrum exhibits three absorption bands centered at 252, 286 and 610 nm, being the latter the characteristic absorption related to the indigoid group (NHC≡CNH) [63–66]. After 60 min of the UV irradiation, the three bands have vanished following a homogenous intensity drop, which suggests that the indigoid group was destroyed until to carboxylic acid without the persistence of the known chromophoric (benzene ring) intermediate products of the IC dye [65,67]. This is confirmed, because the spectra do not show any isosbestic point and the band centered at 195 nm, which initially decreased showed a slight increase after 30 min and decreased again after that (see enlarged area in Fig. 12a). This 195 nm band is due to carboxylic acids that are formed from the degradation of the secondary products of the IC dye, which can only occur by the action of hydroxyl radicals. Therefore under UV irradiation, the large and efficient mineralization percentage (50%) is explained because the intermediate products were immediately mineralized to CO_2.

On the other hand, Fig. 12b shows the absorbance spectrum of the IC dye solution as a function of visible-light irradiation time. As the irradiation time increases, the characteristic peak at 610 nm (and the 286 nm band) slowly decreases, indicating again the destruction of the indigoid group; however, there is a huge increment in the absorbance band at low-wavelengths, now centered at 200 nm (enlarged area Fig. 12b) and the presence of an isosbestic point at 244 nm. The presence of the isosbestic point suggests the formation of others oxidized secondary products occurring during the degradation of the IC dye in solution (2-amine-5-sulfo-benzoic acid, 2,3-dioxo-14-indole-5 sulfonic acid and 2 amino-a-oxo-5-sulfo-benzeneacetic acid) [65,66,68], which persistent in the solution. These secondary products are originated because the indigoid group is primarily broken through reactions with superoxide radicals ($O_2^{\bullet-}$), and they were not immediately degraded into carboxylic acid because the superoxide radicals have not enough oxidizing power, as has been already suggested by some authors [65,66,68]. The elevated absorption centered at 200 nm is mainly caused by the persistent benzene groups of secondary products formed

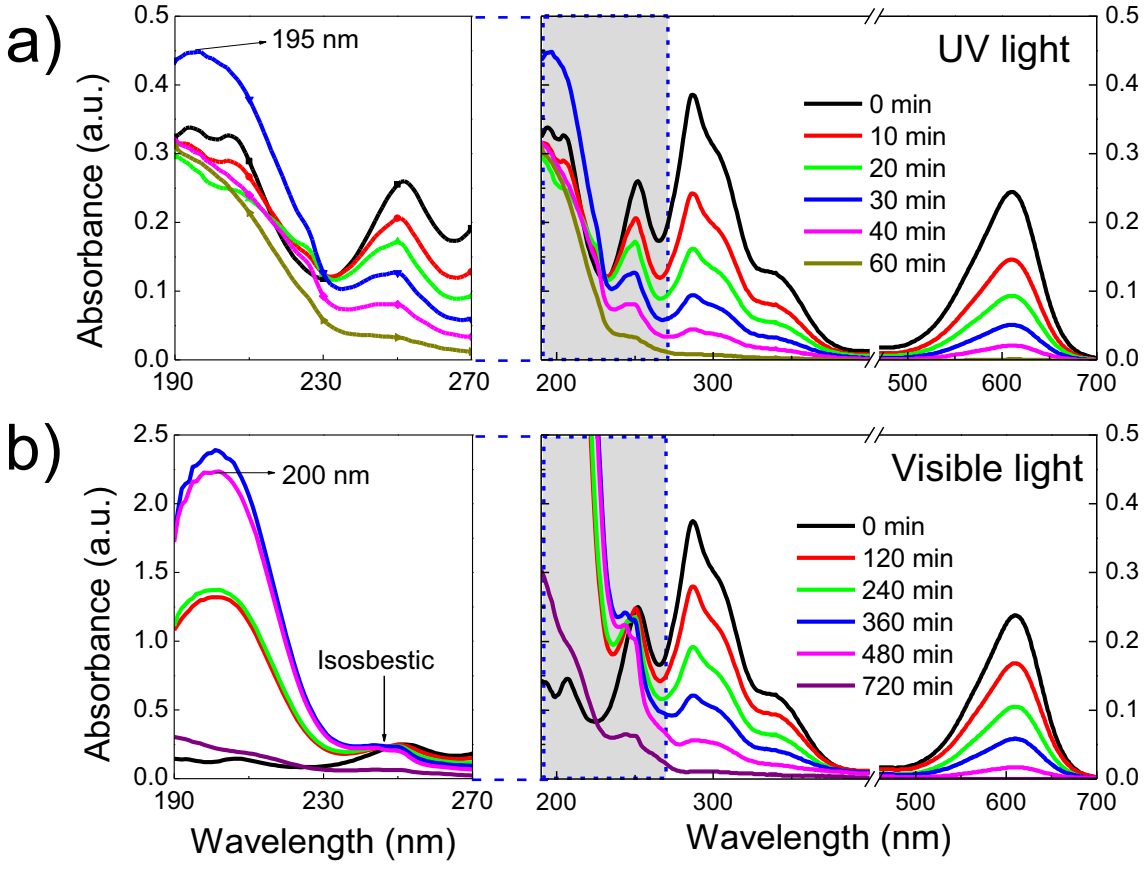

Fig. 12. Evolution of the absorbance spectra of the aqueous solution of IC as a function of irradiation time for different lights a) under UV light b) under visible light.

during the first 480 min of illumination [68]. Similar spectra were observed during the photodegradation of the IC dye using pure ZnO films under visible-light (not shown), confirming that in such case, the photocatalytic reaction occurs via the superoxide radicals.

The high intensity of the chromophoric intermediate products suggest a large fraction of them in the solution which can be explained because the superoxide radicals have not enough power to oxidize the secondary products; they need to interact with hydroxyl radicals on the film surface in order to be decomposed. However, as far as there are still IC dye molecules in the solution, both the adsorption of secondary products and the transformation of superoxide radicals to hydroxyl radicals are limited and so the secondary products remained longer time in the solution. Nonetheless, after 720 min of visible-light irradiation both the isosbestic point at 244 nm disappeared and the absorbance peak at 200 nm decreased, suggesting that those secondary products were converted to carboxylic acid and continue to be mineralized to CO_2 by the already formed powerful hydroxyl radicals. Therefore, under visible-light irradiation, the degradation of the IC dye occurs in two steps: firstly, IC dye is degraded by superoxide radicals forming secondary products, and then, the secondary products are degraded by hydroxyl radicals forming carboxylic acid and later mineralization to CO_2, which is in agreement with the obtained mineralization percentage (43%) in 720 min.

5. Conclusion

In summary, a ZnO/Bi_2O_3 heterojunction was successfully obtained in form of thin film using two simple deposition steps. The ZnO/Bi_2O_3 heterojunction exhibited an excellent photocatalytic performance for the IC degradation under UV irradiation that was mainly driven by the ZnO. However, under visible light illumination, ZnO was not as effective as the ZnO/Bi_2O_3 heterostructure; the photocatalytic activity of ZnO was significantly improved with the coupling to the Bi_2O_3 dots, attaining a superior mineralization degree (43% vs. 17%) due to the strong absorption of the visible light driven by the Bi_2O_3 and the effective separation of the photoinduced e^--h^+ pairs. In the heterojunction, it was found that the degradation using UV light occurs via the ·OH radicals created by the holes in the ZnO-VB, while under the visible light, the degradation is driven by the production of superoxide radicals by the electrons in the CB of both oxides, so different degradation mechanisms of the IC molecule were observed depending on the illumination.

Acknowledgements

This investigation work was funded by the CONACYT-Project (No. 251279) and UNAM PAPIIT IN108618 and IN100116. A. H-G kindly acknowledged to CONACYT for the Catedra-Conacyt/1169 project. Finally, the authors recognized the support of Adriana Tejeda, Omar Novelo, Josué Romero and Dr. E. Rivera for making possible the different measurements.

References

[1] Lee KM, Lai CW, Ngai KS, Juan JC. Recent developments of zinc oxide based photocatalyst in water treatment technology: a review. Water Res 2016;88:428–48.
[2] Lam S-M, Sin J-C, Abdullah AZ, Mohamed AR. Degradation of wastewaters containing organic dyes photocatalysed by zinc oxide: a review. Desalination Water Treat 2012;41(1–3):131–69.
[3] Ma W, Ren B, Huang Z, Chen Q, Cao X, Guo Y. Mesostructured zinc oxide architectures with high photocatalytic activity. Mater Chem Phys 2017;186:341–52.
[4] Di Mauro A, Fragalà ME, Privitera V, Impellizzeri G. ZnO for application in photocatalysis: from thin films to nanostructures. Mater Sci Semicond Process 2017;69:44–51.
[5] Yi Z, Luo J, Ye X, Yi Y, Huang J, Yi Y, et al. Effect of synthesis conditions on the growth of various ZnO nanostructures and corresponding morphology-dependent photocatalytic activities. Superlattice Microst 2016;100:907–17.
[6] Rashid J, Barakat MA, Salah N, Habib SS. ZnO-nanoparticles thin films synthesized by RF sputtering for photocatalytic degradation of 2-chlorophenol in synthetic wastewater. J Ind Eng Chem 2015;23:134–9.
[7] Fageria P, Gangopadhyay S, Pande S. Synthesis of ZnO/Au and ZnO/Ag nanoparticles and their photocatalytic application using UV and visible light. RSC Adv 2014;4(48):24962–72.
[8] Ong WL, Natarajan S, Kloostra B, Ho GW. Metal nanoparticle-loaded hierarchically assembled ZnO nanoflakes for enhanced photocatalytic performance. Nanoscale 2013;5(12):5568–75.
[9] Dorraj M, Alizadeh M, Sairi NA, Basirun WJ, Goh BT, Woi PM, et al. Enhanced visible light photocatalytic activity of copper-doped titanium oxide–zinc oxide heterojunction for methyl orange degradation. Appl Surf Sci 2017;414:251–61.
[10] Senthil Kumar P, Selvakumar M, Ganesh Babu S, Induja S, Karuthapandian S. CuO/ZnO nanorods: an affordable efficient p-n heterojunction and morphology dependent photocatalytic activity against organic contaminants. J Alloy Comp 2017;701:562–73.
[11] Xiuquan G, Cuiyan L, Shuai Y, Mingguo M, Yinghuai Q, Jiefang Z. ZnO based heterojunctions and their application in environmental photocatalysis. Nanotechnology 2016;27(40):402001.
[12] Yan YH, Zhou ZX, Cheng Y, Qiu LL, Gao CP, Zhou JG. Template-free fabrication of alpha- and beta-Bi2O3 hollow spheres and their visible light photocatalytic activity for water purification. J Alloy Comp 2014;605:102–8.
[13] Wang Y, Zhao JZ, Zhou B, Zhao X, Wang ZC, Zhu YC. Three-dimensional hierarchical flowerlike microstructures of alpha-Bi2O3 constructed of decahedrons and rods. J Alloy Comp 2014;592:296–300.
[14] Schlesinger M, Weber M, Schulze S, Hietschold M, Mehring M. Metastable beta-Bi2O3 nanoparticles with potential for photocatalytic water purification using visible light irradiation. Chemistryopen 2013;2(4):146–55.
[15] Ho CH, Chan CH, Huang YS, Tien LC, Chao LC. The study of optical band edge property of bismuth oxide nanowires alpha-Bi2O3. Opt Express 2013;21(10):11965–72.
[16] Medina JC, Bizarro M, Silva-Bermudez P, Giorcelli M, Tagliaferro A, Rodil SE. Photocatalytic discoloration of methyl orange dye by delta-Bi2O3 thin films. Thin Solid Films 2016;612:72–81.
[17] Sammes NM, Tompsett GA, Nafe H, Aldinger F. Bismuth based oxide electrolytes - structure and ionic conductivity. J Eur Ceram Soc 1999;19(10):1801–26.
[18] Cornei N, Tancret N, Abraham F, Mentre O. New epsilon-Bi2O3 metastable polymorph. Inorg Chem 2006;45(13):4886–8.
[19] Gualtieri AF, Immovilli S, Prudenziati M. Powder X-ray diffraction data for the new polymorphic compound omega-Bi2O3. Powder Diffr 1997;12(2):90–2.
[20] Hernandez-Gordillo A, Medina JC, Bizarro M, Zanella R, Monroy BM, Rodil SE. Photocatalytic activity of enlarged microrods of alpha-Bi2O3 produced using ethylenediamine-solvent. Ceram Int 2016;42(10):11866–75.
[21] Liu XJ, Pan LK, Li JL, Yu K, Sun Z. Visible light-induced photocatalytic activity of Bi2O3 prepared via microwave-assisted method. J Nanosci Nanotechnol 2013;13(7):5044–7.
[22] Cheng HF, Huang BB, Lu JB, Wang ZY, Xu B, Qin XY, et al. Synergistic effect of crystal and electronic structures on the visible-light-driven photocatalytic performances of Bi2O3 polymorphs. Phys Chem Chem Phys 2010;12(47):15468–75.
[23] Balachandran S, Swaminathan M. Facile fabrication of heterostructured Bi2O3-ZnO photocatalyst and its enhanced photocatalytic activity. J Phys Chem C 2012;116(50):26306–12.
[24] Iyyapushpam S, Nishanthi ST, Padiyan DP. Photocatalytic degradation of methyl orange using alpha-Bi2O3 prepared without surfactant. J Alloy Comp 2013;563:104–7.
[25] Hou JG, Yang C, Wang Z, Zhou WL, Jiao SQ, Zhu HM. In situ synthesis of alpha-beta phase heterojunction on Bi2O3 nanowires with exceptional visible-light photocatalytic performance. Appl Catal B Environ 2013;142:504–11.
[26] Barrera-Mota K, Bizarro M, Castellino M, Tagliaferro A, Hernandez A, Rodil SE. Spray deposited beta-Bi2O3 nanostructured films with visible photocatalytic activity for solar water treatment. Photochem Photobiol Sci 2015;14(6):1110–9.
[27] Medina JC, Bizarro M, Gomez CL, Depablos-Rivera O, Mirabal-Rojas R, Monroy BM, et al. Sputtered bismuth oxide thin films as a potential photocatalytic material. Catal Today 2016;266:144–52.
[28] Fan HT, Pan SS, Teng XM, Ye C, Li GH, Zhang LD. delta-Bi2O3 thin films prepared by reactive sputtering: fabrication and characterization. Thin Solid Films 2006;513(1–2):142–7.
[29] Xiang QJ, Yu JG, Wong PK. Quantitative characterization of hydroxyl radicals produced by various photocatalysts. J Colloid Interface Sci 2011;357(1):163–7.
[30] Sirota B, Reyes-Cuellar J, Kohli P, Wang L, McCarroll ME, Aouadi SM. Bismuth oxide photocatalytic nanostructures produced by magnetron sputtering deposition. Thin Solid Films 2012;520(19):6118–23.
[31] Malathy P, Vignesh K, Rajarajan M, Suganthi A. Enhanced photocatalytic performance of transition metal doped Bi2O3 nanoparticles under visible light irradiation. Ceram Int 2014;40(1):101–7.
[32] Wu YC, Chaing YC, Huang CY, Wang SF, Yang HY. Morphology-controllable Bi2O3 crystals through an aqueous precipitation method and their photocatalytic performance. Dyes Pigments 2013;98(1):25–30.
[33] Shan LW, Wang GL, Li D, San XY, Liu LZ, Dong LM, et al. Band alignment and enhanced photocatalytic activation of alpha/beta-Bi2O3 heterojunctions via in situ phase transformation. Dalton Trans 2015;44(17):7835–43.
[34] Balachandran S, Swaminathan M. Facile fabrication of heterostructured Bi2O3–ZnO photocatalyst and its enhanced photocatalytic activity. J Phys Chem C 2012;116(50):26306–12.
[35] Wang X, Ren P, Fan H. Room-temperature solid state synthesis of ZnO/Bi2O3 heterojunction and their solar light photocatalytic performance. Mater Res Bull 2015;64:82–7.
[36] Yang Y, Xu L, Su C, Che J, Sun W, Gao H. Electrospun ZnO/Bi2O3 nanofibers with

enhanced photocatalytic activity. J Nanomater 2014;2014:7.
[37] Ling B, Sun XW, Shen YQ, Dong ZL. Hierarchical ZnO/Bi2O3 nanostructures: synthesis, characterization, and electron-beam modification. Appl Phys A 2009;98(1):91.
[38] Li C, Zhang J, Yang Ja, Wang T, Lv X, Tang Z. Methods to improve the photocatalytic activity of immobilized ZnO/Bi2O3 composite. Appl Catal Gen 2011;402(1–2):80–6.
[39] Portillo-Velez NS, Bizarro M. Sprayed pyrolyzed ZnO films with nanoflake and nanorod morphologies and their photocatalytic activity. J Nanomater 2016;2016:1–11.
[40] Dutta DP, Roy M, Tyagi AK. Dual function of rare earth doped nano Bi2O3: white light emission and photocatalytic properties. Dalton Trans 2012;41(34):10238–48.
[41] Wu SX, Fang JZ, Xu XX, Liu Z, Zhu XM, Xu WC. Microemulsion synthesis, characterization of highly visible light responsive rare earth-doped Bi2O3. Photochem Photobiol 2012;88(5):1205–10.
[42] Zhang X, Ai ZH, Jia FL, Zhang LZ, Fan XX, Zou ZG. Selective synthesis and visible-light photocatalytic activities of BiVO4 with different crystalline phases. Mater Chem Phys 2007;103(1):162–7.
[43] Muruganandham M, Amutha R, Lee GJ, Hsieh SH, Wu JJ, Sillanpaa M. Facile fabrication of tunable Bi2O3 self-assembly and its visible light photocatalytic activity. J Phys Chem C 2012;116(23):12906–15.
[44] Wang WJ, Chen XQ, Liu G, Shen ZR, Xia DH, Wong PK, et al. Monoclinic dibismuth tetraoxide: a new visible-light-driven photocatalyst for environmental remediation. Appl Catal B Environ 2015;176:444–53.
[45] Gomez CL, Depablos-Rivera O, Medina JC, Silva-Bermudez P, Muhl S, Zeinert A, et al. Stabilization of the delta-phase in Bi2O3 thin films. Solid State Ionics 2014;255:147–52.
[46] Gomez CL, Rodil SE. High stability and ac-conductivity of cubic fluorite-Bi2O3 films synthesized by magnetron sputtering. Solid State Ionics 2017;309:100–9.
[47] Natsume Y, Sakata H, Hirayama T. Low-temperature electrical conductivity and optical absorption edge of ZnO films prepared by chemical vapour deposition. Phys Status Solidi 1995;148(2):485–95.
[48] Pradhan P, Alonso JC, Bizarro M. Photocatalytic performance of ZnO: Al films under different light sources. Int J Photoenergy 2012;2012:1–7.
[49] Srivastav S, Kumar CVRV, Mansingh A. Effect of oxygen on the physical parameters of Rf sputtered Zno thin-film. J Phys D Appl Phys 1989;22(11):1768–72.
[50] Xu Y, Schoonen MAA. The absolute energy positions of conduction and valence bands of selected semiconducting minerals. Am Mineral 2000;85(3–4):543–56.
[51] Fan HT, Pan SS, Teng XM, Ye C, Li GH. Structure and thermal stability of delta-Bi2O3 thin films deposited by reactive sputtering. J Phys D Appl Phys 2006;39(9):1939–43.
[52] Rauf MA, Ashraf SS. Fundamental principles and application of heterogeneous photocatalytic degradation of dyes in solution. Chem Eng J 2009;151(1–3):10–8.
[53] Rauf MA, Ashraf S, Alhadrami SN. Photolytic oxidation of coomassie brilliant blue with H2O2. Dyes Pigments 2005;66(3):197–200.
[54] Guan HM, Zhu LH, Zhou HH, Tang HQ. Rapid probing of photocatalytic activity on titania-based self-cleaning materials using 7-hydroxycoumarin fluorescent probe. Anal Chim Acta 2008;608(1):73–8.
[55] Zhang J, Nosaka Y. Quantitative detection of OH radicals for investigating the reaction mechanism of various visible-light TiO2 photocatalysts in aqueous suspension. J Phys Chem C 2013;117(3):1383–91.
[56] Naseri A, Samadi M, Mahmoodi NM, Pourjavadi A, Mehdipour H, Moshfegh AZ. Tuning composition of electrospun ZnO/CuO nanofibers: toward controllable and efficient solar photocatalytic degradation of organic pollutants. J Phys Chem C 2017;121(6):3327–38.
[57] Karmakar K, Sarkar A, Mandal K, Khan GG. Stable and enhanced visible-light water electrolysis using C, N, and S Surface functionalized ZnO nanorod photoanodes: engineering the absorption and electronic structure. Acs Sustain Chem Eng 2016;4(10):5693–702.
[58] Herrmann J-M. Heterogeneous photocatalysis: fundamentals and applications to the removal of various types of aqueous pollutants. Catal Today 1999;53(1):115–29.
[59] Foote CS, Valentine JS, Greenberg A, Liebman JF. Active oxygen in chemistry. Structure energetics and reactivity in chemistry series (SEARCH series) 2. Dordrecht: Springer Netherlands; 1996. p. 1. online resource (352 pages).
[60] Brandt C, Vaneldik R. Transition-metal-catalyzed oxidation of sulfur(Iv) oxides - atmospheric-relevant processes and mechanisms. Chem Rev 1995;95(1):119–90.
[61] Davis EA, Mott NF. Conduction in non-crystalline systems V. Conductivity, optical absorption and photoconductivity in amorphous semiconductors. Phil Mag: J Theor Exp Appl Phys 1970;22(179):0903–22.
[62] Chen XQ, Wu ZS, Liu DD, Gao ZZ. Preparation of ZnO photocatalyst for the efficient and rapid photocatalytic degradation of azo dyes. Nanoscale Res Lett 2017:12.
[63] Sousa MM, Miguel C, Rodrigues I, Parola AJ, Pina F, de Melo JSS, et al. A photochemical study on the blue dye indigo: from solution to ancient Andean textiles. Photochem Photobiol Sci 2008;7(11):1353–9.
[64] Gordon PF, Gregory P. Organic chemistry in colour. Berlin ; New York: Springer-Verlag; 1983.
[65] Coelho MG, de Lima GM, Augusti R, Maria DA, Ardisson JD. New materials for photocatalytic degradation of Indigo Carmine-Synthesis, characterization and catalytic experiments of nanometric tin dioxide-based composites. Appl Catal B Environ 2010;96(1–2):67–71.
[66] Guaraldo TT, Zanoni TB, de Torresi SIC, Goncales VR, Zocolo GJ, Oliveira DP, et al. On the application of nanostructured electrodes prepared by Ti/TiO2/WO3 "template": a case study of removing toxicity of indigo using visible irradiation. Chemosphere 2013;91(5):586–93.
[67] Dalmazio I, de Urzedo APFM, Alves TMA, Catharino RR, Eberlin MN, Nascentes CC, et al. Electrospray ionization mass spectrometry monitoring of indigo carmine degradation by advanced oxidative processes. J Mass Spectrom 2007;42(10):1273–8.
[68] Hernandez-Gordillo A, Rodriguez-Gonzalez V, Oros-Ruiz S, Gomez R. Photodegradation of Indigo Carmine dye by CdS nanostructures under blue-light irradiation emitted by LEDs. Catal Today 2016;266:27–35.